Acta Oceanol. Sin., 2023, Vol. 42, No. 9, P. 1–15
https://doi.org/10.1007/s13131-023-2159-9
http://www.aosocean.com
E-mail: ocean2@hyxb.org.cn

Influence of asymmetric tidal mixing on sediment dynamics in a partially mixed estuary

Zhongyong Yang[1, 2], Zhiming Liang[1, 3], Yufeng Ren[3*], Daobin Ji[1, 2], Hualong Luan[4], Changwen Li[1], Yujie Cui[1], Andreas Lorke[5]

[1] College of Hydraulic and Environmental Engineering, China Three Gorges University, Yichang 443002, China

[2] Hubei Field Observation and Scientific Research Stations for Water Ecosystem in Three Gorges Reservoir, China Three Gorges University, Yichang 443002, China

[3] Hubei Key Laboratory of Intelligent Yangtze and Hydroelectric Science, China Yangtze Power Co., Ltd., Yichang 443000, China

[4] River Research Department, Changjiang River Scientific Research Institute, Wuhan 430010, China

[5] Institute for Environmental Sciences, University of Koblenz-Landau, Landau 76829, Germany

Received 27 August 2022; accepted 4 November 2022

© Chinese Society for Oceanography and Springer-Verlag GmbH Germany, part of Springer Nature 2023

Abstract

To investigate the influence of asymmetric tidal mixing (ATM) on sediment dynamics in tidal estuaries, we developed a vertically one-dimensional idealized analytical model, in which the M_2 tidal flow, residual flow and suspended sediment concentration (SSC) are described. Model solutions are obtained in terms of tidally-averaged, and tidally-varying components (M_2 and M_4) of both hydrodynamics and sediment dynamics. The effect of ATM was considered with a time-varying eddy viscosity and time-varying eddy diffusivity of SSC. For the first time, an analytical solution for SSC variation driven by varying diffusivity could be derived. The model was applied to York River Estuary, where higher (or lower) eddy diffusivity was observed during flood (or ebb) in a previous study. The model results agreed well with the observation in both hydrodynamics and sediment dynamics. The vertical sediment distribution under the influence of ATM was analyzed in terms of the phase lag of the M_2 component of SSC relative to tidal flow. The phase lag increases significantly in estuaries with typical ATM (higher diffusivity during flood and lower diffusivity during ebb) for the case of seaward-directed net bottom shear stress (e.g., strong river discharge). In contrary, the phase lag is reduced by ATM, if the tidally-averaged bottom shear stress is landward (e.g., strong horizontal density gradient). The dynamics of sediment transport was analyzed as a function of ATM phase lag to identify the time of highest sediment diffusivity, as well as a function of the residual flow, to evaluate the relative importance of seaward and landward residual flows. In estuaries with relative strong fresh water discharge or weak tidal forcing (in case of flood season or neap tide), the near bottom SSC could be higher during ebb than during flood, since the bottom shear stress is higher during ebb due to seaward residual flow. However, landward net sediment transport can be expected in these estuaries in case of a typical ATM, because higher diffusivity causes higher SSC and landward transport during the flood period, while both SSC and seaward transport could be lower during ebb. On the contrary, seaward sediment transport can be expected in estuaries with landward tidally mean bottom shear stress in case of a reverse ATM, where sediment diffusivity is higher during the ebb.

Key words: idealized model, asymmetric sediment diffusivity, vertical sediment phase lag, sediment transport

Citation: Yang Zhongyong, Liang Zhiming, Ren Yufeng, Ji Daobin, Luan Hualong, Li Changwen, Cui Yujie, Lorke Andreas. 2023. Influence of asymmetric tidal mixing on sediment dynamics in a partially mixed estuary. Acta Oceanologica Sinica, 42(9): 1–15, doi: 10.1007/s13131-023-2159-9

1 Introduction

Estuarine turbulence is characterized by high rates of kinetic energy dissipation rate and strong vertical density stratification or buoyancy frequency with both extending to much higher values than in other natural environments (Geyer et al., 2008). The asymmetric variations of hydrodynamics and sediment transport during flood and ebb periods are ubiquitous in estuaries. Mechanistic understanding of the asymmetries of hydrodynamics and sediment dynamics is important because the characteristics of sediment distributions and transport have a profound influence on harbor silting (Jiang et al., 2013), pollutant transport (Tessier et al., 2011), as well as on geomorphological evolution (Luan et al., 2017).

Asymmetry of hydrodynamics during a tidal period includes several aspects, such as peak current asymmetry, slack water asymmetry, and asymmetric tidal mixing (ATM). The latter is

Foundation item: The National Natural Science Foundation of China under contract Nos U2040220, 52079069, 52009066, 52379069, 52009079, 42006156 and U2240220; the CRSRI Open Research Program under contract No. CKWV20221003/KY; the Open Research Program of Hubei Key Laboratory of Intelligent Yangtze and Hydroelectric Science under contract No. ZH2102000109; the Outstanding Young and Middle-aged Scientific and Technological Innovation Team in Universities of Hubei Province under contract No. T2021003; the Hubei Province Chutian Scholar Program (granted to Andreas Lorke).
*Corresponding author, E-mail: ren_yufeng@ctg.com.cn

controlled by tidal straining, which is the semidiurnal variation in thermohaline stratification induced by the interaction of the vertically sheared tidal currents with the along-estuary salinity gradient (Simpson et al., 1990). Field measurements in many partially mixed estuaries demonstrated that tidal straining typically promotes vertical mixing during the flood tide and stratification during ebb, such as in the Liverpool Bay (Simpson et al., 1990), Columbia River Estuary (Jay and Musiak, 1994), Hudson River Estuary (Scully and Geyer, 2012; Geyer and MacCready, 2014) and York River Estuary (Scully and Friedrichs, 2007). Similar results for semidiurnal variations of mixing and stratification were obtained from a numerical model of a partially mixed estuary (Cheng et al., 2011). However, reverse asymmetry of tidal mixing with enhanced stratification during flood and intensified mixing during the ebb phase have also been examined (Fugate et al., 2007). Similar observations have been made in estuaries with a side embayment freshwater source (Lacy and Monismith, 2001; Fram et al., 2007) or with a significant variation of lateral bathymetry (Cheng and Wilson, 2008; Li et al., 2015).

The residual flow induced by ATM could be solved analytically (Jiang et al., 2013) or decomposed from numerical results (Chen and De Swart, 2018; Cheng et al., 2019). The strength and vertical structure of ATM-induced flow are associated to distinct estuarine mixing types. According to the numerical study of Cheng et al. (2011, 2013), the ATM induced flow has a two layer structure similar to that of density driven flow in weakly stratified estuaries. In partially mixed and highly stratified estuaries, it tends to have a three-layer structure of residual flow, with landward flows near the surface and bottom, and seaward flow in the middle of the water column (Cheng et al., 2011). In addition, the strength of ATM induced flow is positively correlated to the degree of vertical mixing (Cheng et al., 2013). These arguments are consistent with observations (Stacey et al., 2010; Cheng et al., 2020) and results from analytical models (Jiang et al., 2013).

The variation of vertical mixing and stratification between flood and ebb periods not only affects vertical residual circulation, but also the suspended sediment load (Scully and Friedrichs, 2007; Dijkstra et al., 2017). Tidal straining of the horizontal density gradient causes a stronger pycnocline lower in the water column, which acts as a barrier for sediment resuspension and reduces eddy diffusivity by limiting turbulent length scales during the ebb period (Geyer and MacCready, 2014; Li et al., 2018). This process is accounted for by modifying the value of eddy diffusivity based on the gradient Richardson number (Friedrichs and Hamrick, 1996). The observation in the York River Estuary showed that, higher values of eddy viscosity would occur during the less stratified flood period due to tidal straining. As a result, more sediment become re-suspended during the flood period and the net sediment transport is directed landward, despite of a net seaward advective flux with approximately equal current magnitude and shear (Scully and Friedrichs, 2003). The reverse asymmetry of sediment diffusivity is also observed in some other estuaries, e.g., the Changjiang River Estuary, where the stratification was strengthened during the flood tide and weakened during the ebb tide, with the control of the advection of the salt wedge (Li et al., 2015). The asymmetry of diffusivity induced suspended sediment transport, which is a part of tidal pumping transport, is likely important for the fine sediment movement in partially mixed estuaries (Uncles et al., 2006; Burchard et al., 2018). For silt-sized sediment particles, the numerical results of Geyer et al. (1997) indicated a 20-fold increase in the sediment transportation rate with inclusion of the mixing/stratification effect on turbulent sediment diffusion. With a semi-analytical model (iFlow model), Dijkstra et al. (2017, 2019) showed that the time-varying eddy viscosity and sediment diffusivity may have a similar important contribution on both tidal flow (traditional ATM) and gravitational circulation (eddy viscosity-shear covariance, or ESCO).

In summary, the residual flow induced by asymmetric eddy viscosity has been widely observed and studied using numerical and analytical models. Observations also indicated that the time varying diffusivity may be important for the sediment distribution and transport. However, accurate simulation of suspended sediment concentration (SSC) are subject to limitations, such as temporal variations of bed roughness, settling velocity, eddy diffusivity, which constrain mechanistic understanding of the effects of ATM on sediment dynamics.

In this paper, a vertical one-dimensional idealized model is developed to examine the influence of ATM on SSC and sediment transport in estuaries. Although the rigorous model assumptions are challenged by the complex estuarine hydrodynamics and sediment dynamics, the idealized model could be solved analytically and facilitates mechanistic understanding by isolating the individual mechanisms. In this study, analytical solutions are obtained for the main component of tidal flow (M_2) and for the residual flow, as well as for the mean and tidally varying components of SSC. The main objectives of this study are: (1) to examine the vertical structure of ATM-induced SSC; (2) to analyze the time lag between ATM-induced mixing and corresponding changes in the vertical distribution of SSC; (3) to discuss the importance of ATM-induced changes in SSC on sediment transport. The paper is structured as follows: the model and the solution technique are introduced in Section 2; in Section 3, we apply the model to a specific case study (the York River Estuary) and compare model results with observations taken from literature; further analyses of model results are presented in Section 4, followed by a discussion in Section 5 and conclusions in Section 6.

2 Analytical model

2.1 *Hydrodynamics*

We describe the vertical (z, unit: m) distribution of the along-estuary (x, unit: m) velocity ($u(z)$) using the one-dimensional (vertical) shallow water equation in an Cartesian coordinate system (x, z):

$$\frac{\partial u}{\partial t} = \frac{g}{\rho_0}\frac{\partial \rho}{\partial x}z - g\frac{\partial \eta}{\partial x} + \frac{\partial}{\partial z}\left(A\frac{\partial u}{\partial z}\right), \tag{1}$$

where the x-axis points from land to sea and the z-axis points vertically upward, with $z = 0$ at the undisturbed water surface (Fig. 1). u is the along-estuary velocity (unit: m/s), t is time (unit: s), $g \approx 9.81$ m/s^2 is gravitational acceleration, $\rho_0 \approx 1\,020$ kg/m^3 is the reference water density and $\partial\eta/\partial x$ represents the water level gradient (unit: 1). The along-estuary density gradient ($\partial\rho/\partial x$) is prescribed and assumed to be constant (Chernetsky et al., 2010). The vertical eddy viscosity coefficient A (unit: m^2/s) is assumed to be constant over depth and varies during the tidal cycle as a cosine function (Cheng et al., 2010),

$$A = A_0 + A_2 = A_0 + |A_2|\cos(\omega t - \theta), \tag{2a}$$

where A_0 represents a constant (tidal mean) part and $|A_2|$ is the amplitude of the tidal varying part, which is proportional to and an order smaller than the mean part, ($|A_2| = \alpha A_0$). ω (unit: s^{-1}) is the M_2 tidal frequency and θ (unit: 1) is the phase angle of A_2. It

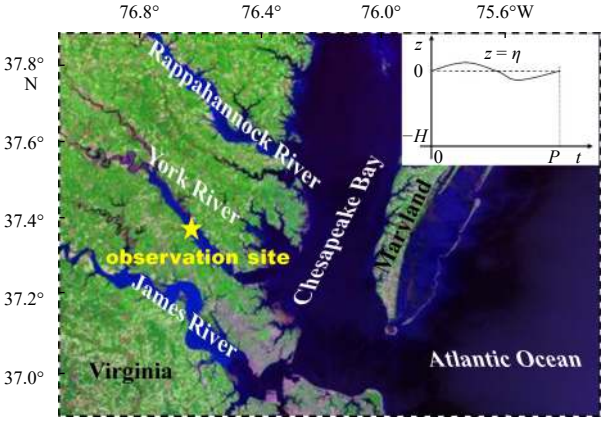

Fig. 1. Site map of the York River Estuary showing the location of field observations. A sketch map of the model geometry attached in the top-right corner, where $z=\eta$ is the elevation of the water surface and $z=-H$ is the bed. The horizontal dashed line indicates the average sea level ($z=0$), while the solid line shows surface elevation during a tidal period of length P.

should be noted that eddy viscosity is affected by the magnitude of the tidal velocity and by the vertical density stratification. Under the influence of the former, the eddy viscosity would vary at the M_4 frequency, since it is high during both flood maxima and ebb maxima, hence the frequency doubled. However, many observations and numerical studies found a typical semi-diurnal variation (M_2 frequency) of eddy viscosity over a tidal cycle, which results from the influence of density stratification (Stacey et al., 2008; Cheng et al., 2020). Therefore, we only considered variations at the M_2 frequency in this model. The mean part of vertical eddy viscosity coefficient (A_0) is parameterized using the formulation of Munk and Anderson (1948) with $A_0=c_V U(H/2)(1+10Ri)^{-1/2}$. In this expression, c_V is an empirical coefficient, $Ri=g(\Delta\rho/\rho)(H/2)/U^2$ is the depth-averaged bulk Richardson number, H is the water depth, $\Delta\rho$ is the residual bed to surface density difference and U is a typical value of the current velocity, which is assumed to be equal to the amplitude of the tidal velocity. An external semidiurnal tidal discharge q_2 (unit: m²/s) and a constant river discharge q_0 are imposed,

$$\int_{-H}^{0} u\mathrm{d}z = q_0 + q_2. \tag{2b}$$

The imposed semidiurnal tidal discharge $q_2=q_{2a}\cos(\omega t)$ has an amplitude (q_{2a}) and with the M_2 tidal frequency (ω). The kinematic boundary conditions at the sea surface is applied,

$$A\frac{\partial u}{\partial z}=0, \text{at } z=\eta. \tag{2c}$$

At the riverbed $z=-H$, partial slip and impermeability condition are imposed (Chernetsky et al., 2010),

$$A\frac{\partial u}{\partial z}=su, \text{ at } z=-H, \tag{2d}$$

where the parameter s is the constant partial slip parameter.

2.2 *Sediment dynamics*

SSC (c, unit: kg/m³) is described by the one-dimensional (vertical) advection-diffusivity equation,

$$\frac{\partial c}{\partial t}+\frac{\partial}{\partial z}\left(w_s c-K\frac{\partial c}{\partial z}\right)=0. \tag{3}$$

The settling velocity (w_s) is assumed to be constant, as its variation over a tidal cycle is small for estuaries with relative low SSC (Manning and Bass, 2006). The sediment vertical eddy diffusivity (K, unit: m²/s) varies during the tidal cycle with the same scaling coefficient as eddy viscosity ($K_2=\alpha|K_0|$) and the same phase value θ. Here we assume a same proportional coefficient (α) and phase lag value (θ) for eddy diffusivity (K) and eddy viscosity (A), since both are influenced by the tidal varying structure of mixing and stratification. Strong (weak) stratification during ebb (flood) indicates both low (high) eddy viscosity and eddy diffusivity. Hence,

$$K=K_0+K_2=K_0+|K_2|\cos(\omega t-\theta), \tag{4a}$$

with $K_0=c_V U_2(H/2)(1+3.33Ri)^{-1/2}$ denoting the mean component of sediment vertical eddy diffusivity. At the water surface, the diffusive and settling sediment flux balance,

$$w_s c+K\frac{\partial c}{\partial z}=0, \text{ at } z=\eta, \tag{4b}$$

where both the diffusive flux $\left(K\frac{\partial c}{\partial z}\right)$ and settling flux ($w_s c$) are positive since we use a positive value of settling velocity, although it should be negative in our coordinate system. A normal flux condition is imposed at the bottom,

$$w_s c_a+K\frac{\partial c}{\partial z}=0, \text{ at } z=-H, \tag{4c}$$

where c_a is the dimensionless reference sediment concentration and it is parameterized as (Dyer, 1997)

$$c_a=a\rho_s\frac{(1-p)}{\tau_c}|\tau_b(t)|, \tag{4d}$$

In this expression, $\rho_s\approx 2\,650$ kg/m³ is the sediment density, $p\approx 0.4$ is the porosity of the sediment, a indicates the amount of sediment at the bed available for resuspension, τ_c is the threshold bed shear stress, and τ_b is the bed shear stress, which defined as

$$|\tau_b|=\rho_0 A\left|\frac{\partial u}{\partial z}\right|, \text{ at } z=-H, \tag{4e}$$

where $|\cdot|$ denotes the absolute value.

2.3 *Analytical solutions*

The governing equations of flow and SSC are solved analytically with perturbation techniques, in which the physical components are divided into several order of magnitudes (Huijts et al., 2006). During perturbation analysis, the governing equations are non-dimensionalized firstly. Then we introduced a small parameter ($\varepsilon\ll 1$) to indicate the order of each terms in the governing equations. In this process, we assumed that the values of some terms are significant smaller (or an order smaller) than other terms (e.g., $\varepsilon=\frac{u_0}{u_2}\ll 1$ means the residual flow u_0 is an order

lower than the tidal flow u_2). All model assumptions are summarized in Table 1. They have been used in related studies, and are validated using observations for typical tidal estuaries (Huijts et al., 2006; Jiang et al., 2013).

With scaling analysis and perturbation analysis, the governing equations and boundary conditions can be decomposed into separate equations for tidal flow (u_2), residual flow ($u_0 = u_{0\rho} + u_{0a} + u_{0q}$), tidally-averaged SSC (c_0), M_2 SSC variations ($c_2 = c_{2t} + c_{2a}$) and M_4 SSC variations (c_4), which can be solved analytically. Here, c_{2t} is driven by the rectification and bottom shear stress from residual flow, while c_{2a} depicts the part of sediment vertical diffusion induced by the time-varying diffusivity $\left(\text{i.e., } K_2\frac{\partial^2 c_0}{\partial z^2}\right)$. At last, the vertical profile of sediment flux per unit width ($F = F_0 + F_2 = F_{0\rho} + F_{0a} + F_{0q} + F_{2t} + F_{2a}$, unit: kg/(m²·s)) is obtained as the mean product (uc) over a tidal cycle (P). The sediment transport per unit width ($T = T_0 + T_2 = T_{0\rho} + T_{0a} + T_{0q} + T_{2t} + T_{2a}$, unit: kg/(m·s)) is obtained by integrating the vertical profile of sediment flux over depth. All symbols introduced above are described in Table 2. As for the subscripts used during this process, numbers indicate the fluctuation frequency, while letters (if exist) indicate the physical driving force. Therefore, (u_0, u_2) denote residual flow and M_2 tidal flow, while $(u_{0a}, u_{0q}, u_{0\rho})$ denote residual flow driven by asymmetric tidal mixing, by fresh water discharge, and by the along-estuary density gradient, respectively. A detailed description of the decomposition is described in Appendix A.

3 Field data

To compare the analytical model to observations, we used field data from the York River Estuary, Virginia, reported in a study by Scully and Friedrichs (2003). The York River Estuary is a sub-estuary of the west Chesapeake Bay. Most of the estuary has a main channel with maximum depth reaching 10 m and is flanked by two shallow shoals. The typical tidal range is about 0.7 m, with a typical tidal current reaching 1.0 m/s during spring. The average river discharge is about 31 m³/s. The estuary is partially mixed, but tidal asymmetries in salinity stratification were found to play an important role in vertical momentum transfer and sediment suspension, and to have a great influence on sediment transport (Lin and Kuo, 2001). The tidal velocity and SSC were recorded with an acoustic Doppler current profiler and an optical backscatter sensor for about 25 h in April 1999. Detailed information of the observation can be found in Scully and Friedrichs (2003). The parameter values applied in the analytical model are either taken from Scully and Friedrichs (2003, 2007), or deduced from the study results of these two studies (Table 3). For example, the ratio $|K_2|/K_0$ (i.e., $\alpha = 0.3$) and the phase lag (i.e., $\theta = 1.4\pi$) are estimated from the variation of eddy viscosity depicted in the reference study (Scully and Friedrichs, 2003, 2007). In addition, the selected model input parameters (marked with asterisks in Table 3) were adjusted to obtain best agreement of the model results with observation.

4 Results

4.1 *Model application to York River Estuary*

4.1.1 *Hydrodynamics*

The simulations of the York River Estuary for the period of ob-

Table 1. Assumptions of the one-dimensional analytical model

Assumption	Explanation
$\frac{\eta}{H} = O(\varepsilon)$	water level fluctuation is an order of magnitude smaller than water depth
$\left(\frac{U_0}{U_2}, \frac{U_d}{U_2}, \frac{U_q}{U_2}\right) = O(\varepsilon)$	residual currents are an order of magnitude smaller than tidal currents
$\left(\frac{A}{\omega H^2}, \frac{K}{\omega H^2}\right) = O(1)$	frictional force can affect the whole water column
$\left(\frac{A_2}{A_0}, \frac{K_2}{K_0}\right) = O(\varepsilon)$	the fluctuating component of eddy viscosity (diffusivity) is an order of magnitude smaller than the mean component
$\frac{w_s}{\omega H} = O(1)$	length scale of sediment settling during a tidal cycle is comparable to water depth

Note: Here, (U_0, U_2) represent typical values of the mean velocity and M_2 tidal velocity, respectively. The parameters $U_d = gH^3\left(\frac{\partial \rho}{\partial x}\right)/(48\rho A)$ and $U_q = 2q/(3H)$ are the typical velocity scales for residual currents driven by an along-estuary density gradient and fresh water discharge. The parameter $\varepsilon \ll 1$ indicates the magnitude of the difference to higher-order physical components.

Table 2. Definition of symbols used in the model description

Symbol	Definition	Symbol	Definition
ω	M_2 tidal frequency	w_s	settling velocity
P	M_2 tidal period	c	SSC
Ri	Richardson number	c_0	tidally mean SSC (dominant order)
s	partially slip parameter	c_4	M_4 component SSC (dominant order)
$\partial\rho/\partial x$	along-estuary density gradient	c_2	M_2 component SSC (first order)
q_0	fresh water discharge	c_{2t}	bottom shear stress induced c_2
q_2	M_2 tidal discharge	c_{2a}	ATM induced c_2
u	along-estuary velocity	c_a	reference concentration
u_2	M_2 tidal velocity (dominant order)	(A, K)	eddy viscosity and eddy diffusivity
u_0	tidally mean velocity (first order)	(A_0, K_0)	tidally mean component of A and K
u_{0a}	ATM induced u_0	(A_2, K_2)	M_2 component of A and K
$u_{0\rho}$	$\partial\rho/\partial x$ induced u_0	$(\|A_2\|, \|K_2\|)$	amplitude of A_2 and K_2
u_{0q}	fresh water discharge induced u_0	θ	phase of A_2 or K_2

Note: ATM: asymmetric tidal mixing; SSC: suspended sediment concentration.

Table 3. Model input parameter values representative for a point in the York River Estuary, USA during April 1999 (referenced from Scully and Friedrichs (2003, 2007))

Quantity	Symbol	Value
Water depth	H	7.0 m
Amplitude of tidal velocity	U_2	0.6 m/s
Depth mean velocity	U_0	0.045 m/s
Angular M_2 tidal frequency	ω	1.4×10^{-4} s^{-1}
Gravitational acceleration	g	9.81 m/s^2
Reference density	ρ_0	1 020 kg/m^3
*Bed to surface density difference	$\Delta\rho$	2.0 kg/m^3
*Along-channel density gradient	$\partial\rho/\partial x$	8.6×10^{-4} kg/m^4
*Threshold bed shear stress	τ_c	0.002 kg/(m·s^2)
*Settling velocity	w_s	0.6 mm/s
*Ratio of $\lvert K_2\rvert/K_0$ or $\lvert A_2\rvert/A_0$	α	0.3
*Phase lag of K_2 or A_2	θ	1.4π

Note: The stars mark the parameters deduced from the above references and were modified during model validation.

servations reported in Scully and Friedrichs (2003) covered two semi-diurnal tidal cycles (the observation lasted 25 h) (Fig. 2). The current velocity during flood period (negative values) and ebb period (positive values) were nearly equal since the semi-diurnal tidal current was the dominant flow (Fig. 2a). In reality, the ebb current was slightly stronger in the upper water column, while the flood current was slightly stronger in the lower part of the water column (Fig. 2b). For the mean flow, the up-estuary velocity (negative values) in the lower part of the water column was mainly contributed by the flow component driven by the longitudinal density gradient ($u_{0\rho}$), while the downstream velocity (positive values) in the upper water column was mainly contributed by freshwater discharge (u_{0q}). The component of the mean flow induced by ATM (u_{0a}) had a nearly identical vertical structure as $u_{0\rho}$, which is consistent with the analytical results of Jiang et al. (2013) for the North Passage of the Changjiang River Estuary with a same θ value. According to the study of Cheng et al. (2010), the vertical structure of u_{0a} is a function of θ. However, the relative contribution of u_{0a} is not as significant as reported in former studies (Stacey et al., 2010; Burchard and Hetland, 2010; Jiang et al., 2013), since the strength of u_{0a} is highly correlated to the degree of mixing and stratification (Cheng et al., 2013). According to the study of Scully and Friedrichs (2003), the York River Estuary is partially mixed, the ratio of $\lvert K_2\rvert/K_0$ ($\alpha\approx0.3$) is relative small. The horizontal shift between observed mean flow and model results can be attributed to the ignored components of residual flow in our model, such as Stokes return flow, which drives a residual current to one direction over the whole depth.

4.1.2 *Sediment dynamics*

The model results of vertical-temporal variation of SSC over two tidal periods showed that, SSC attained maximal values during both flood and ebb maxima in flow magnitude (Fig. 2). Hence, dominant variations in SSC occurred at a frequency of 2ω, which is mainly accounted for by the M_4 component SSC (c_{4t} in Fig. 3e). The M_2 component of SSC can be driven by the rectification and bottom shear stress from residual flow (c_{2t} in Fig. 3c) and advection of time-varying diffusivity with vertical shear of mean SSC (i.e., $K_2\dfrac{\partial^2 c_0}{\partial z^2}$, c_{2a} in Fig. 3d). The component c_{2t} was positive (negative) during flood (ebb) period since the near bottom residual flow was landward (Fig. 2b). The component c_{2a} was positive during flood slack period since the phase lag of K_2 was 1.4π (i.e., highest diffusivity occurs during flood slack). Both observation and model results showed that, the near bottom SSC was significantly higher during flood period than that during ebb period (Figs 3a, b). Our model decomposition results reveal that the higher near bottom SSC during flood could mainly be attributed to c_{2t}. High values of c_{2a} were concentrated in middle layer, which can be also deduced from the vertical distribution of amplitude of each component (Fig. 3f).

4.1.3 *Sediment flux*

The vertical distribution of sediment flux is shown in Fig. 4. In correspondence to residual flows, the residual sediment flux induced by u_{0a} (F_{0a}) and $u_{0\rho}$ ($F_{0\rho}$) is landward, while that induced by u_{0q} (F_{0q}) is seaward. The tidal flux related to c_{2t} (F_{2t}) is landward. With the similar explanation as for c_{2a}, the tidal flux related to c_{2a} (F_{2a}) is seaward. Although the maximum value of c_{2t} (~ 40 g/m^3, Fig. 3c) is significantly larger than that of c_{2a} (~ 28 g/m^3, Fig. 3d), the corresponding sediment fluxes (F_{2t} and F_{2a}) are of comparable magnitude, since that the higher values of c_{2a} mainly occurred in the middle or upper water column, where current velocity was high. As for the component F, both the observation and model results indicate the values of F is positive (seaward) in the upper water column and negative (landward) at lower depth. The

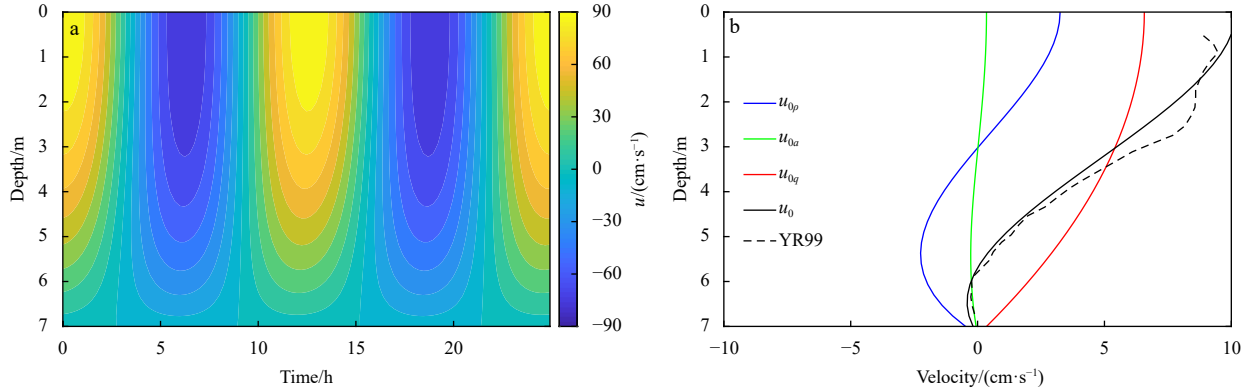

Fig. 2. Model results of the vertical-temporal structure of total flow velocity ($u=u_0+u_2$) (a) and of the vertical structure of the residual components (b) based on the parameters of an observation point in the York River Estuary (Table 1). The blue line shows the flow component driven by the longitudinal density gradient ($u_{0\rho}$), the green line is contribution of asymmetric tidal mixing (u_{0a}), and the red line is the contribution from fresh water discharge (u_{0q}). The solid black line shows the corresponding modeled mean velocity and the dashed line shows the observed mean velocity from Scully and Friedrichs (2003).

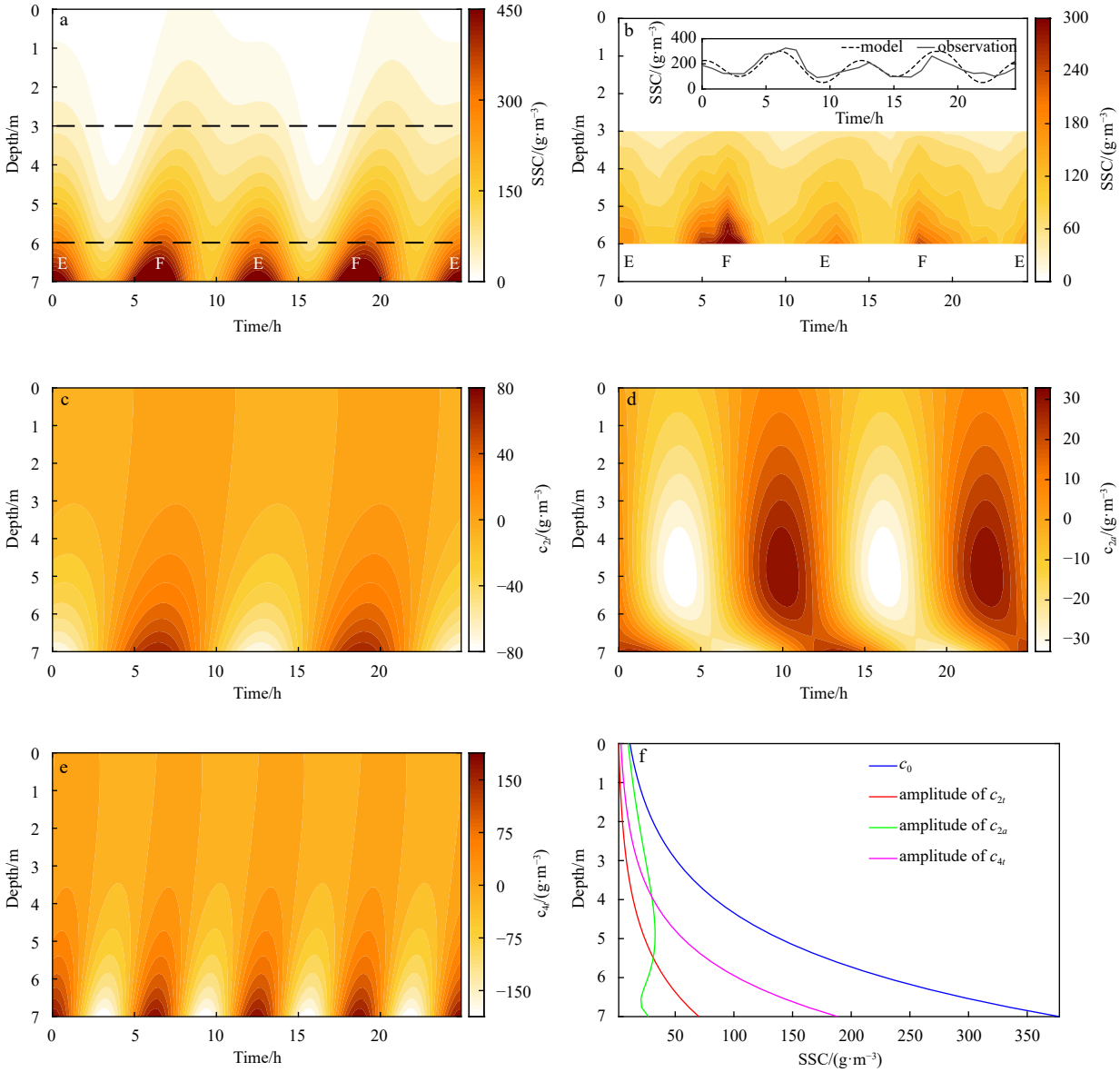

Fig. 3. Model results (a) and observations (b, taken from Scully and Friedrichs (2003)) for the vertical-temporal structure of suspended sediment concentration (SSC) over two M_2 tidal periods (~ 25 h). The line plots in panel b compares temporal variation of near bottom SSC (z = 7 m) from observations and model results. The dashed horizontal lines in panel a mark the depth range with observational data shown in panel b. The labels "F" and "E" in panel a and b denote "flood" and "ebb", respectively. Panels c, d and e show individual components of M_2 component SSC induced by bottom shear stress (c_{2t}), M_2 component SSC induced by asymmetry of diffusivity (c_{2a}), and M_4 component SSC induced by bottom shear stress (c_{4t}), respectively. Panel f shows the vertical distribution of SSC amplitude of each component.

positive seaward flux in the upper water column was mainly contributed by F_{2a}, while the negative landward flux in the lower water column were contributed from mutual effect of F_{2a} and $F_{0\rho}$.

4.2 *Effect of asymmetric tidal diffusivity on vertical sediment distribution*

The model results in Section 4.1 showed that, the high values of ATM-induced variations in SSC (c_{2a}) is concentrated on the vertical middle depth with high tidal flow velocity, while the high values of SSC component induced by the near bottom shear stress of tidal flow (c_{2t}) occurs at the near bottom area with low tidal flow velocity. Thus the sediment flux of F_{2a} ($F_{2a} = \langle u_2 c_{2a} \rangle$) is considerable to that of F_{2t} ($F_{2t} = \langle u_2 c_{2t} \rangle$), even though the absolute value of c_{2a} is smaller than that of c_{2t} (Fig. 3). Many estuaries are well mixed during the flood period and stratified during the ebb period (typical ATM). The occurrence of reverse tidal asymmetry was attributed to a number of reasons, including a freshwater source from a side embayment (Fram et al., 2007), or lateral straining effect on deep-shoal system (Cheng et al., 2011). To consider both types of asymmetries, we varied the phase angle of K_2 (θ) between 0 and 2π. We considered four specific cases in which $\theta = [0, 0.5\pi, \pi, 1.5\pi]$ represent highest vertical diffusion coefficient occurs at the period of ebb maxima, ebb slack, flood maxima and flood slack, respectively (Fig. 5). The structure of c_{2a} shifts gradually in time when the value θ varies from 0 to 2π. A small phase lag (about 1 h) between maximum values of K_2 and highest concentration c_{2a} was caused by the time required for resuspension and vertical transport of sediment. In the following

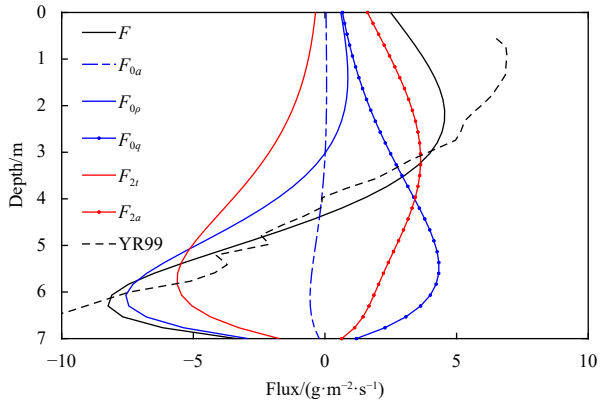

Fig. 4. Vertical structure of sediment flux and its components based on the parameters for a point in the York River Estuary. F_{0a}, $F_{0\rho}$ and F_{0q} represent residual sediment flux related to asymmetry tidal eddy viscosity, horizontal density gradient, and river discharge. F_{2t} and F_{2a} represent tidal sediment flux related to bottom shear stress varying in M_2 frequency and asymmetry tidal diffusivity. The dashed black line (YR99) shows the observed sediment flux cited from Scully and Friedrichs (2003).

subsections, the vertical structure of SSC under the influence of ATM will be examined firstly in dependence on the phase lag. Following that, the relationship between the phase angle of K_2 and sediment flux will be discussed.

In a tidal estuary, the amplitude of SSC variation decreases with height above the bed (i.e., amplitude attenuation). In addition, the response of SSC to the tidal current is not instantaneous, and the SSC variation lags behind the velocity (i.e., phase lag ϕ) due to adjustment of the balance between upward diffusion and downward settling of sediment particles. In the study of Yu et al. (2011), the vertical distribution of the phase lag $\phi(z)$ between variations in SSC and tidal flow was analytically derived as

$$\phi(z) = \frac{w_s}{K}\sqrt{\frac{1+\sqrt{1+16\omega^2K^2/w_s^4}}{8}}. \tag{5}$$

In their study, this analytical solution assumed a constant value of K, i.e., the component c_{2a} resulting from ATM was neglected. Besides, the bottom SSC was prescribed rather than driven by bed shear stress. However, our model results showed that, the time-varying sediment diffusivity have a significant influence on sediment vertical distribution (Fig. 5). Furthermore, the variation of bed shear stress highly depends on the residual flow. Here, we discuss the vertical phase lag based on two residual flow scenarios, i.e., (i) $\partial\rho/\partial x = 0$, $U_0 = 0.10$ m/s and (ii) $\partial\rho/\partial x = 1\times10^{-3}$ kg/m^4, $U_0 = 0$. The first scenario represents a strongly stratified estuary, while the second scenario represents a fully mixed estuary. In these two scenarios, the near bottom shear stress induced by residual flow, as well as the c_{2t} component (induced by net bottom shear stress), are nearly equivalent. However, the maximum value of near bottom shear stress occurs at flood period in scenario (i), while it occurs at ebb period in scenario (ii). It will be shown that the influence of c_{2a} on these two scenarios is quite different.

In agreement with the solution proposed by Yu et al. (2011), the tidal-driven component SSC predicted by our model showed an increasing phase lag for increasing distance above the bed (Fig. 6a). Except for the near-surface region, there was good

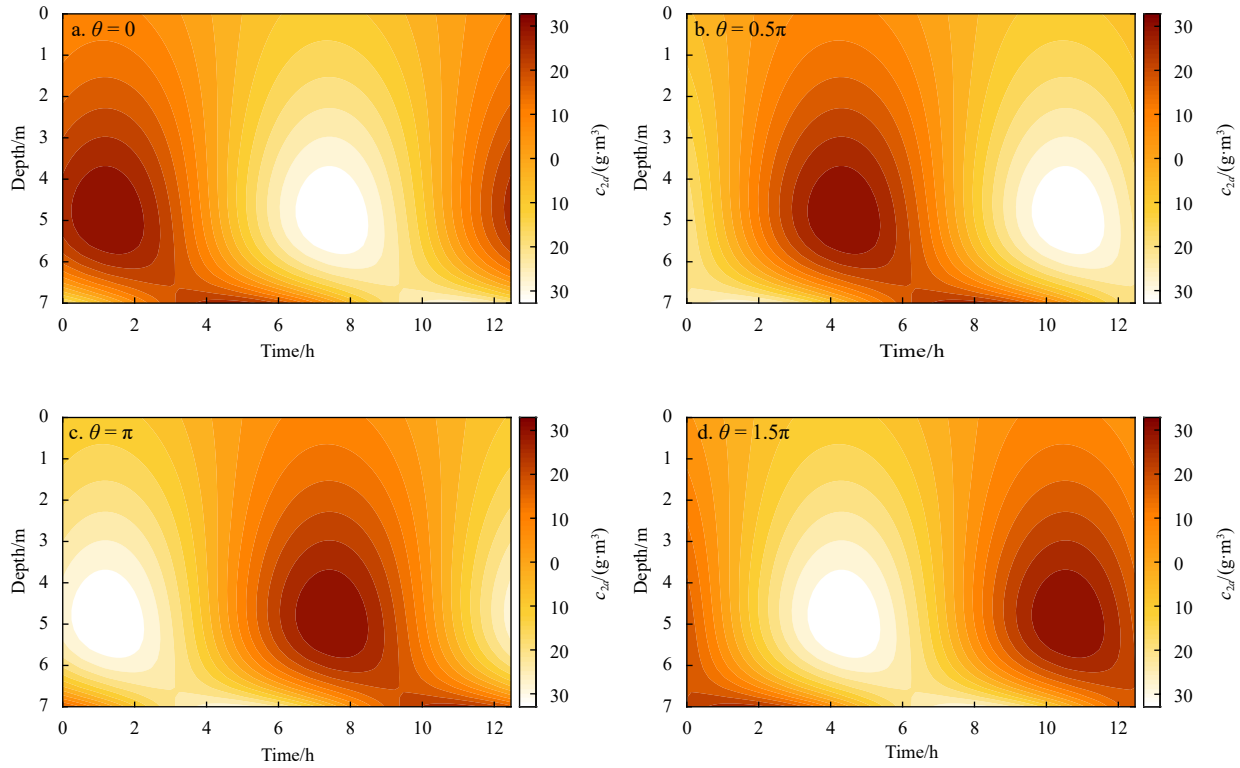

Fig. 5. Vertical-temporal structure of the asymmetric tidal mixing (ATM)-induced SSC (c_{2a}) during a single M_2 tidal period for different phase angles between tidal flow and sediment diffusivity (θ). Panels a, b, c and d represent $\theta = 0, \theta = 0.5\pi$, $\theta = \pi$ and $\theta = 1.5\pi$, respectively. The remaining parameters are shown in Table 1.

agreement between both our model results and Yu et al. (2011) (gray line compares to black line in Fig. 6). Taking the effect of the ATM-induced SSC (c_{2a}) into account, the vertical profile of the phase lag of c_2 ($c_2 = c_{2a} + c_{2t}$) changes dramatically in dependence on the phase of sediment diffusivity (θ).

In the first residual flow scenario ($\partial\rho/\partial x = 0, U_0 = 0.15$ m/s), bottom shear stress is higher during the ebb period compared to the flood period, thus the c_{2t} component is positive (negative) during ebb (flood). Considering the influence of c_{2a}, if $\theta = 0$, maximum diffusivities occurred during ebb, thus c_{2a} is positive during ebb (Fig. 5a). c_{2a} did not change the vertical profile of $\phi(z)$ too much (red lines compared to gray line in Fig. 6a). However, the occurrence of the maximum value of c_{2a} was gradually delayed for increasing θ (Fig. 5), which results in a gradually increasing phase lag of c_2. The positive values of c_{2a} occur during the flood period in case of $\theta = \pi$ (Fig. 5c), because of the higher sediment diffusivity. As a result, the vertical distribution of the phase lag of c_2 differs far strongly from that of c_{2t} (cyan lines compared to gray line in Fig. 6a). The temporal and vertical distribution of the M_2 component of SSC (c_2) under four θ values $(0, 0.5\pi, \pi, 1.5\pi)$ in case of ($\partial\rho/\partial x = 0, U_0 = 0.15$ m/s) are shown in Fig. 7, where the vertical distribution of the phase lag can easily be observed.

In the second residual flow scenario ($\partial\rho/\partial x = 1\times10^{-3}$ kg/m^4, $U_0 = 0$), the near bottom shear stress and the c_{2t} component were positive (negative) during the flood (ebb) period, since the residual shear stress induced by the density gradient is directed landward, thereby enhancing the flood current. In this residual case, if $\theta = \pi$ (maximum diffusivities occur at flood), the c_{2a} component would only increase the value of the M_2 SSC component, but not change its phase, because both c_a and c_{2t} are highest during the flood period. Therefore, the zero phase lag would occur at $\theta = \pi$ (Fig. 6b, cyan line). The temporal and vertical distributions of the M_2 component of SSC (c_2) for four θ values $[0, 0.5\pi, \pi, 1.5\pi]$ for scenario (ii) are shown in Fig. 8.

4.3 *Effect of tidally varying diffusivity on vertical sediment transport*

In tidal estuaries, the residual flow plays an important role in the process of both sediment resuspension and transport. On the one hand, the residual sediment transport is induced by the superposition of residual flow and tidal mean SSC. On the other hand, asymmetry of sediment transport would occur between flood and ebb periods under the influence of residual flow, and thus tidal transport is induced. River discharge and the horizontal density gradient are two important factors for residual flow in estuaries. According to the classification based on salinity structure (Dyer, 1997), high fresh water discharge would make the estuary stratified (e.g., Silver Bay, Alaska), while a strong tide would result in fully mixed conditions (e.g., James River Estuary). In this study, the ratio of the typical residual velocity induced by density gradient and fresh water discharge ($\gamma = [u_{0\rho}] / [u_{0q}]$) is used to quantify the degree of vertical mixing. A higher value of γ indicates a highly mixed estuary while a lower value of γ indicates a strongly stratified estuary. Here square brackets ($[\cdot]$) indicate the velocity scale of residual flow, which is derived from the analytical solutions of Huijts et al. (2009) to estimate the relative importance of the various residual flow mechanisms from estuarine parameters. The velocity scale of density-gradient-driven residual flow ($[u_{0\rho}]$) and discharge-driven residual flow ($[u_{0q}]$) reads,

$$[u_{0\rho}] = \frac{1}{48}\frac{H^3}{A_0}\frac{g}{\rho_0}\frac{\partial\rho}{\partial x}, \tag{6a}$$

$$[u_{0q}] = \frac{3}{2}\frac{q_0}{H}. \tag{6b}$$

The variation of tidally mean bottom shear stress $\langle\tau_b\rangle$ over γ and θ is shown in Fig. 9a. Generally, the value $\langle\tau_b\rangle$ is flood-ward (negative) in estuaries with larger along-estuary density gradients (large γ), while $\langle\tau_b\rangle$ is ebb-ward (positive) in the estuaries with a relative small values of γ (larger scale of river discharge induced flow). It should be noted that, the value of bottom shear stress should be always positive due to its definition, here the positive (or negative) sign indicates the direction of $\langle\tau_b\rangle$, i.e., positive means seaward, negative means landward. Following Fig. 9a, the bottom shear stress (τ_b) is higher in case of density driven flow than that of river discharge driven flow with an equal velocity length scale, as the vertical length scale (z) of the former is much smaller (the solid white line is below the dashed white line in Fig. 9a). In addition, there is a slight variation of $\langle\tau_b\rangle$ when θ increases from 0 to 2π due to the ATM generated residual flow (u_{0a}). The vertical structure of u_{0a} is similar to that of $u_{0\rho}$ for

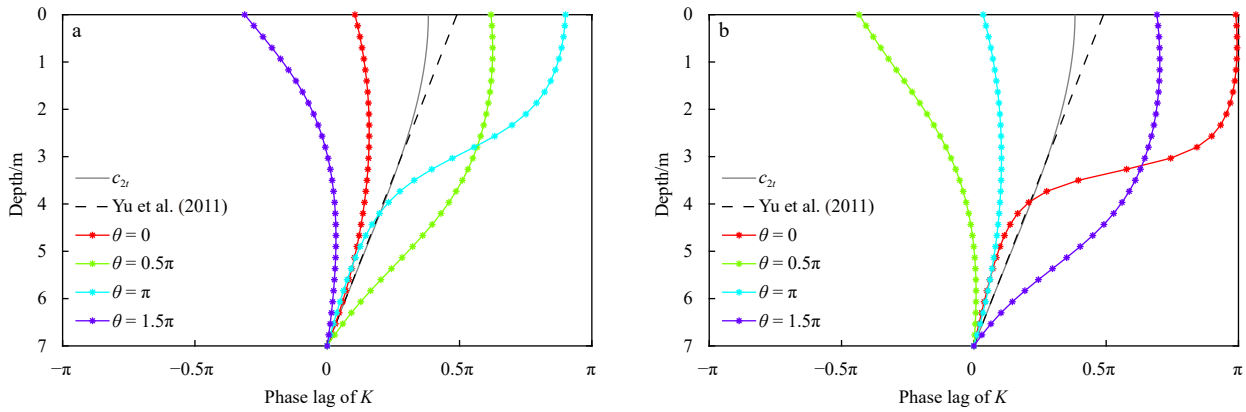

Fig. 6. Vertical structure of phase lag of suspended sediment concentration in response to diffusivity phase θ in case of: $\partial\rho/\partial x = 0, U_0 = 0.15$ m/s (scenario z (i)) (a) and $\partial\rho/\partial x = 1\times10^{-3}$ kg/m^4, $U_0 = 0$ (scenario (ii)) (b). The black line represents the analytical result of Yu et al. (2011). The gray line shows the model results of c_{2t}, i.e., without consideration of asymmetric tidal mixing. The remaining 4 colored lines represent the result of $\phi(z)$ with consideration of c_{2a} for four θ values $(0, 0.5\pi, \pi, 1.5\pi)$.

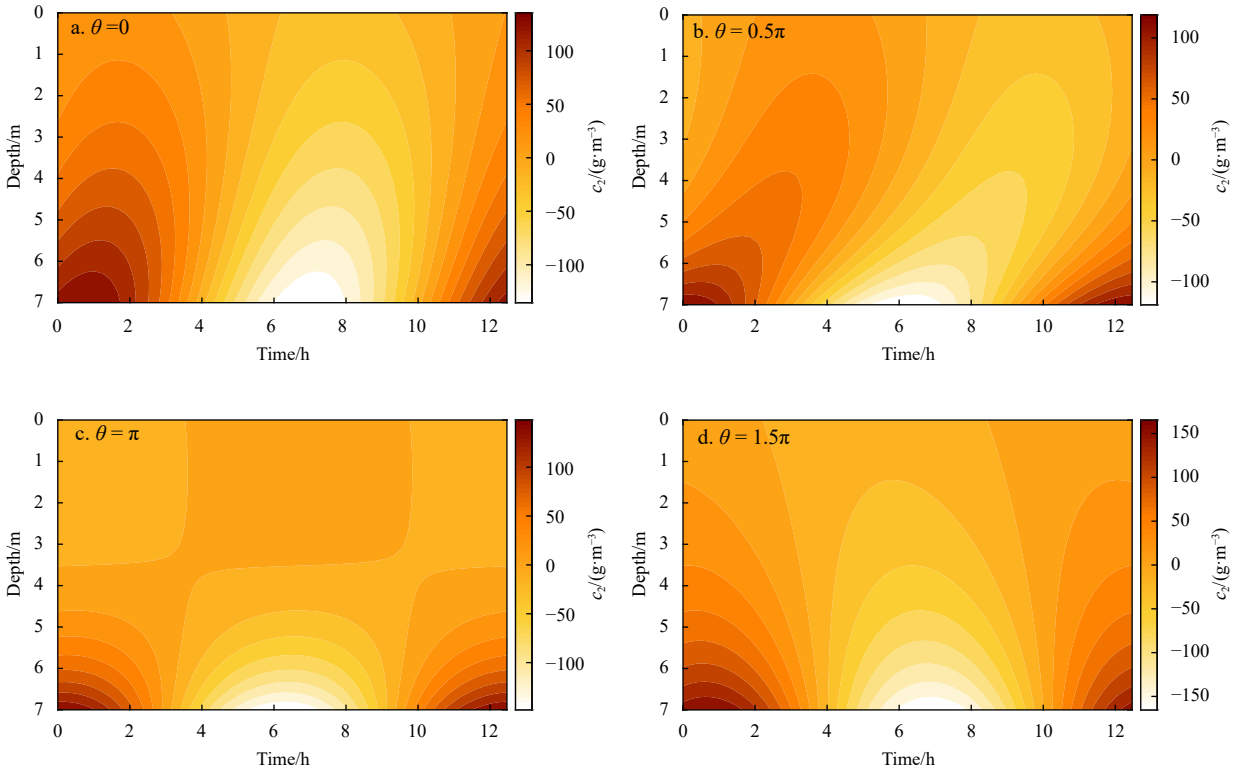

Fig. 7. Vertical structure of M_2 suspended sediment concentration (SSC) component (c_2) over a tidal period under four different values of phase angle of tidally varying sediment diffusivity (θ) in case of scenario (i), $\partial\rho/\partial x = 0$, $U_0 = 0.15$ m/s. Panels a, b, c and d show results for $\theta = 0$, $\theta = 0.5\pi$, $\theta = \pi$ and $\theta = 1.5\pi$, respectively.

$\theta = \pi$, which enhances the flood current over the near bottom area, thus the shear stress $\langle\tau_b\rangle$ attains its maximum value in flood direction under this condition. On the contrary, the near bottom ebb current will be enhanced by u_{0a} during $\theta = 0$ (Cheng et al., 2010), and the shear stress $\langle\tau_b\rangle$ attains its maximum value in ebb direction.

The sediment transport per unit width of the estuary (i.e., the sediment flux) and its components are shown in Figs 9b–i as a function of γ and θ. Generally, the total sediment transport (Fig. 9i) is directed upstream ($T_{ssc} < 0$) in estuaries with a strong density gradient and a weak river discharge ($\gamma > 1$), in which the net bottom shear stress is landward ($\langle\tau_b\rangle < 0$). Contrary, $T_{ssc} > 0$ in the estuaries for which $\gamma < 1$ and $\langle\tau_b\rangle > 0$. However, there is a transitional region for $\theta = 0.5\pi$ to 1.2π, for which the total sediment transport is directed upstream (negative T_{ssc}) despite a net seaward directed bottom shear stress (positive $\langle\tau_b\rangle$). Furthermore, seaward sediment transport can be expected in estuaries with a net upstream directed bottom shear stress for $\theta = 1.2\pi - 2.0\pi$ or $\theta = 0 - 0.5\pi$. The former situation was actually observed in the York River Estuary (Scully and Friedrichs, 2003).

The total sediment transport is composed of residual sediment flux (T_0, Fig. 9g) and the M_2 tidal transport (T_2, Fig. 9h). The zero residual flux line ($T_0 = 0$, red solid line) locates at upward (upward means the direction of higher γ value) of zero bottom shear stress line ($\langle\tau_b\rangle = 0$, white solid line) in Fig. 9g. The main reason could be that, in the estuaries of $\gamma \approx 1$, although the net bottom shear stress generated by $u_{0\rho}$ is stronger than that associated with u_{0q}, the residual sediment flux induced by u_{0q} (T_{0q}) is much higher than that induced by $u_{0\rho}$ ($T_{0\rho}$) (Figs 9c, d). Although the total vertical profile of u_{0q} is directed seaward, half of the vertical profile of $u_{0\rho}$ is landward (Fig. 2b). The residual transport induced by u_{0a} is shown in Fig. 9b, which is relative weak since that u_{0a} is relative weak.

The M_2 tidal transport can be decomposed into two components, T_{2a} and T_{2t} due to that the M_2 component SSC. c_2 is affected by bottom shear stress and by ATM, i.e., $T_2 = T_{2a} + T_{2t}$. The component T_{2t} is driven by the interaction of u_2 and c_{2t}, in which the component c_{2t} is induced by the asymmetry of bed shear stress, thus the zero line of T_{2t} coincide completely with the zero line of $\langle\tau_b\rangle$ (Fig. 9f). The transport component T_{2a} is independent from bottom shear stress or from the scale of residual flow, and only a function of θ. The value of c_{2a} is positive (negative) during flood (ebb) period when $\theta = 0.3\pi - 1.3\pi$ (see Figs 5b and c for $\theta = 0.5\pi$ and π for example), thus the transport component T_{2a} is landward. In contrary, the value of c_{2a} is positive (negative) during ebb (flood) period at the remaining values of θ (see Figs 5a and d for $\theta = 0$ and $\theta = 2\pi$ for example), thus the transport T_{2a} is seaward. In addition, although the typical value of c_{2a} is smaller than that of c_{2t}, the contribution of T_{2a} is significantly larger than that of T_{2t}. This is because the high values of c_{2a} are concentrated on the middle of the water column, where the velocity is relative high, while high values of c_{2t} mainly occur at the near bottom region, where the velocity is relative small. Furthermore, comparing Figs 9e, f and g shows that the component T_{2a} is the key factor for allowing the solid red line and white line to intersect, i.e., the inconsistently direction of net bottom shear stress and total sediment transport.

5 Discussion

5.1 *Effect of ATM on estuarine sediment dynamics*

The vertical structure of tidal flow and SSC was modeled us-

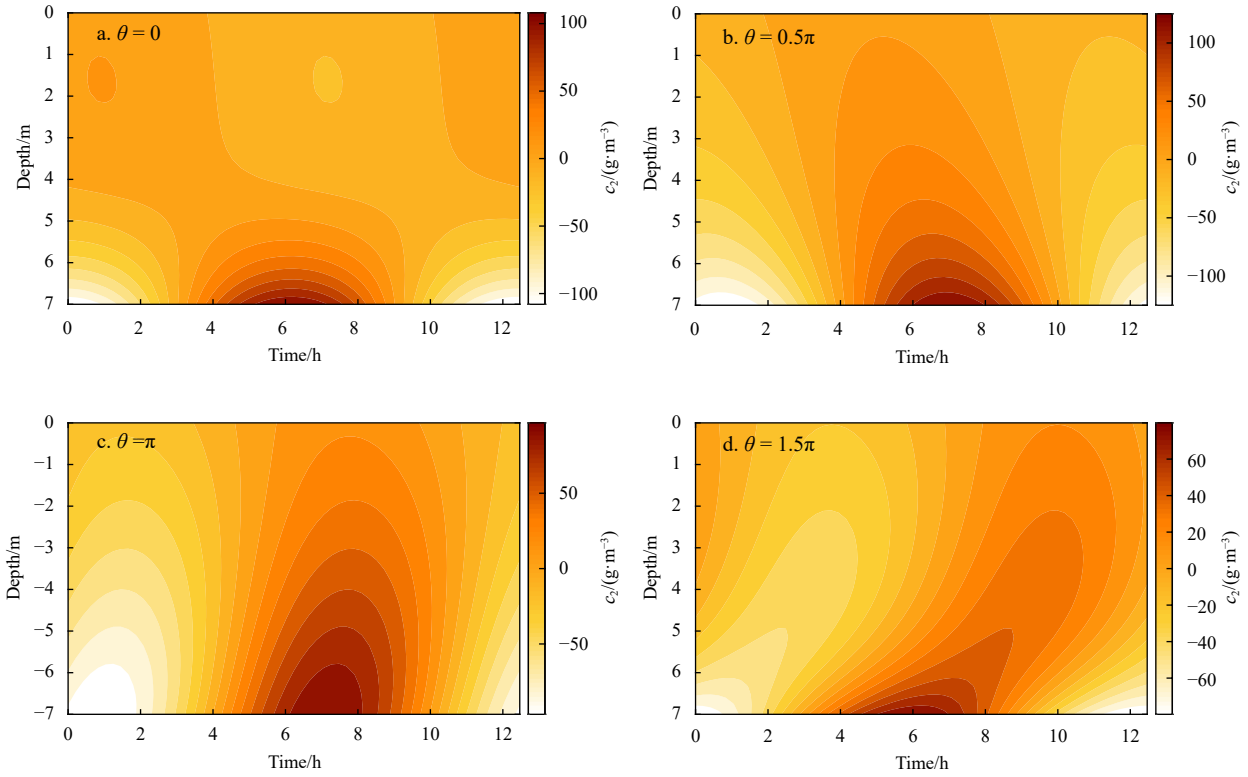

Fig. 8. Vertical structure of M_2 suspended sediment concentration (SSC) component (c_2) over a tidal period under four different values of phase angle of tidally varying sediment diffusivity (θ) in case of scenario (ii), $\partial\rho/\partial x = 1 \times 10^{-3}$ kg/m^4, $U_0 = 0$. Panels a, b, c and d show results for $\theta = 0$, $\theta = 0.5\pi$, $\theta = \pi$ and $\theta = 1.5\pi$, respectively.

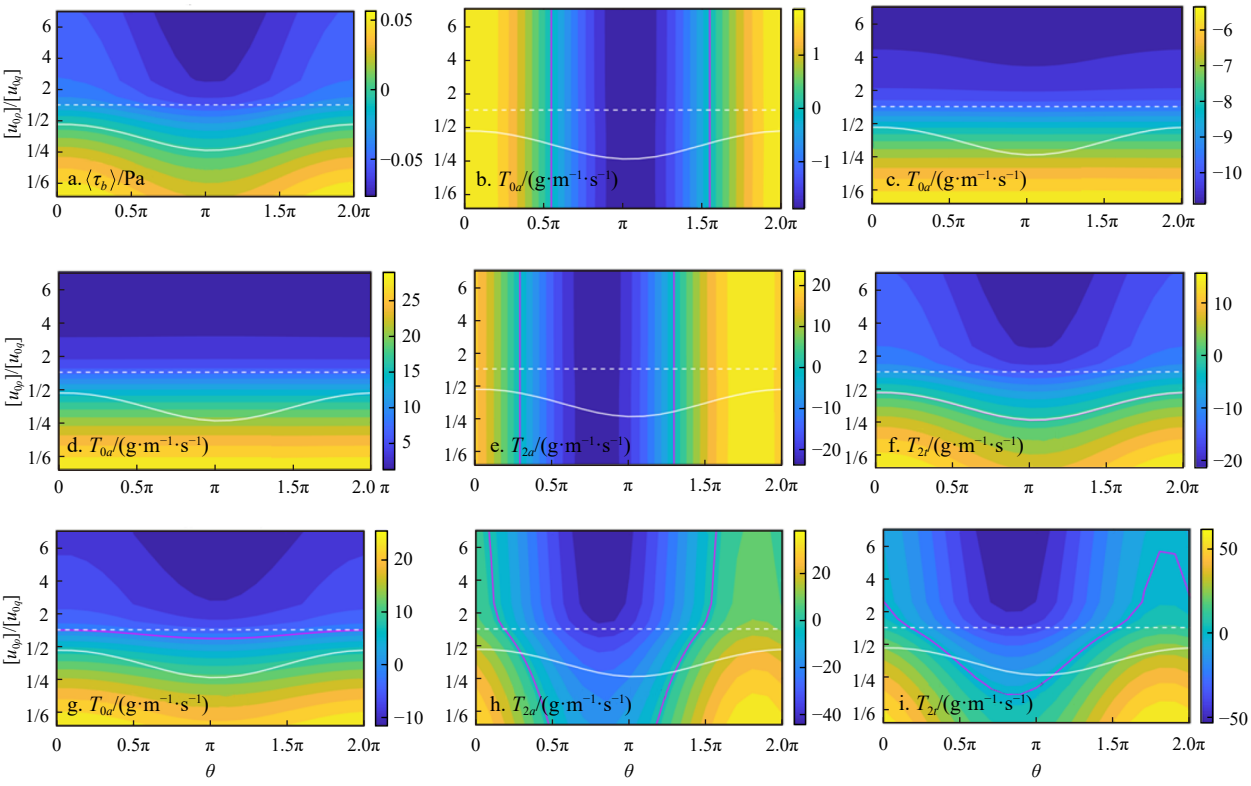

Fig. 9. Tidally mean near bottom shear stress $\langle\tau_b\rangle$ (a) and sediment flux (b–i) as a function of θ and $\gamma = [u_{0\rho}] / [u_{0q}]$. The dashed white line indicates a ratio $\gamma = 1$. The solid white line indicates the value γ for which the average shear stress $\langle\tau_b\rangle = 0$. The solid red line in panel b–i indicates values of γ for which the sediment flux is zero. The remaining boundary conditions can be found in Table 1.

ing a one-dimensional analytical model, with a focus on the asymmetric variation of the sediment diffusion coefficient during a tidal cycle. We analyzed the vertical profile of SSC in terms of the phase lag between temporal variations in SSC and tidal flow. With a one-dimensional analytical model, Yu et al. (2011) solved the vertical profile of the phase lag without consideration of ATM, and suggested that the phase lag of SSC increases linearly from the bottom to the surface (Fig. 6, dashed line). By considering the effects of ATM on sediment diffusion, our model showed that the vertical distribution of the phase lag is strongly influenced by ATM. In estuaries with typical ATM structure (higher diffusivity during flood and lower diffusion during ebb), and with residual flow that is dominated by fresh water discharge (e.g., during the flood season or neap tides), the near bottom SSC is be higher during ebb than that during flood due to higher near bottom shear stress. However, in the upper part of the water column, ATM causes an increased SSC during flood. This result is consistent with observations from the North Passage of the Changjiang River Estuary (Jiang et al., 2013). It has been found that the sediment transport associated with the M_2 tidal flow is landward in some areas, even though the fresh water discharge is quite strong during flood season, which may partly account for severe siltation in this area (Jiang et al., 2013; Wang et al., 2017). Similar observations were made in the York River Estuary (Scully and Friedrich, 2003), where the residual flow and near bottom shear stress was seaward due to river discharge, but SSC was higher during the flood period, bottom shear stress is reduced and the tidal-averaged transport is landward. These observation results are consistent with our model prediction (see Fig. 9h, seaward shear stress corresponds to landward sediment transport).

In estuaries with reverse ATM structure, i.e., higher eddy diffusion occurring during ebb, the sediment diffusion phase lag varies between 0 and 0.5π. This kind of reverse ATM was observed in the two shallow shoals of upper Chesapeake Bay (Fugate et al., 2007), where the vertical distribution of SSC was more uniform during ebb than that during flood, indicating a higher diffusion during ebb and lower diffusion during ebb. The residual flow in the two shoals was seaward under the influence of river discharge according to Huijts et al. (2009). As a result, the SSC in the whole water column was much higher during ebb in response to higher diffusion and bottom shear stress, whereas much lower during flood in response to low diffusion and bottom shear stress. This is consistent with our model shown in Fig. 7a, in particular consistent with the modeled vertical distribution of the phase lag (Fig. 6a, $\theta \approx 0$). Similar reverse ATM structure and SSC variations were also observed in numerical simulations of an idealized estuary (Cheng et al., 2011) and in measurements at the South Channel in the Changjiang River Estuary (Yang et al., 2017).

5.2 *Study limitations*

The model in this paper focused on the vertical distribution of hydrodynamics and sediment dynamics, and provided mechanistic insight into the processes controlling sediment transport in estuaries and identification of their main environmental drivers. However, several factors, which might be important for the asymmetric tidal mixing of sediment diffusion, are not included in this model. First, and most important, our model is one dimensional, which neglects longitudinal and lateral variations and implies a straight channel shape of the estuary. Since we focused on the hydrodynamics and sediment dynamics and their vertical variation at a single location, longitudinal phenomena such as, turbidity maxima and salinity intrusions, could not be considered in this model. Furthermore, in a deep channel and shallow shoal system, the shoals may undergo a reverse tidal asymmetry process due to enhanced stratification by lateral straining during flood, while promoting vertical mixing during ebb (Cheng et al., 2011). Alternatively, the case of reverse tidal asymmetry was considered by the parameters, i.e., vertical eddy viscosity (A) and diffusivity (K). In reality, both parameters (A and K) are a function of salt transport (Cheng et al., 2010) and sediment distribution (Talke et al., 2009), and vary over depth (Chen and de Swart, 2018). Consideration of these dependencies prevents an analytical solution of the model; thus, we followed previous studies (e.g., Chernetsky et al., 2010) and considered them as fixed input parameters. Furthermore, the vertical velocity was ignored ($w = 0$) due to the conservation law (no lateral process and no along-estuary variation of along-estuary velocity, i.e., $v = 0$, $\partial u/\partial x = 0$), which implies the vertical advection term ($w\partial u/\partial z = 0$) was ignored, and the vertical movement of sediment only depends on diffusion and settling velocity. The vertical advection term was an order smaller than the inertia term ($\partial u/\partial t$) according to the scaling analysis (Huijts et al., 2009). The effect of vertical velocity in sediment movement may result higher SSC during flood (upward tidal velocity) and lower SSC during ebb (downward tidal velocity). However, higher settling velocity can be expected due to flocculation process occurred during flood with higher salinity, while lower settling velocity may occur during ebb (Winterwerp, 2002; Dijkstra et al., 2019). These processes were represented by the asymmetry of sediment diffusivity in our model. At last, the sediment transport due to M_4 tidal flow was ignored, even though the M_4 component of SSC is one of the dominant parts of SSC, and M_4 tidal flow could be generated by nonlinear advection terms (Yang et al., 2014), or be amplified in a convergent channel (Friedrichs and Aubrey, 1994). The main reason for that is the lack of M_4 tidal discharge to solve for M_4 tidal flow. Fortunately, the M_4 tidal transport is relatively small as demonstrated in former studies (e.g., Jiang et al., 2013; Yang et al., 2014).

6 Conclusions

In this paper, we investigated the influence of time-varying diffusivity on sediment transport in a tidal estuary with an idealized analytical model. The one-dimensional (vertical) model considered M_2 tidal flow and a residual flow driven by along-estuary density gradient, fresh water discharge, and asymmetric tidal mixing. The suspended sediment concentration and sediment transport were balanced between settling and turbulent diffusion, and was decomposed into a tidal-averaged part and components varying with M_2 frequency and M_4 frequency. For the first time, our analytical model included SSC variations driven by time-varying diffusivity during a tidal cycle. As a case study, we applied the model to York River Estuary, where higher eddy diffusivity during flood and lower diffusivity during ebb were observed in a previous study. The model results agreed well with the observation. With the model, we analyzed the influence of asymmetric tidal mixing on sediment distribution and transport. The vertical distribution of the phase lag between SSC and tidal flow is strongly influenced by the time-varying diffusivity. The phase lag increases in the case of a typical ATM ($\theta \approx \pi$) in an estuary with seaward tidally mean bottom shear stress, where the residual flow is dominated by river discharge. Contrary, the phase lag is reduced by ATM, if the tidally mean bottom shear stress is landward. Also sediment transport is highly dependent

on the direction of bottom shear stress and ATM phase. In estuaries with typical ATM, higher diffusivity during flood results in enhanced landward tidal transport. Net landward sediment transport can be expected under these conditions, even if the net residual flow is seaward for relative high freshwater discharge (e.g., during flood season or neap tide period). On the contrary, in estuaries with relatively strong tides (e.g., during drought season or spring tides), reverse ATM may result in a net seaward sediment transport, even if the gravitational circulation induces a higher near bottom SSC during flood than that during ebb.

References

Burchard H, Hetland R D. 2010. Quantifying the contributions of tidal straining and gravitational circulation to residual circulation in periodically stratified tidal estuaries. Journal of Physical Oceanography, 40(6): 1243–1262, doi: 10.1175/2010JPO4270.1

Burchard H, Schuttelaars H M, Ralston D K. 2018. Sediment trapping in estuaries. Annual Review of Marine Science, 10: 371–395, doi: 10.1146/annurev-marine-010816-060535

Chen Wei, De Swart H E. 2018. Estuarine residual flow induced by eddy viscosity-shear covariance: Dependence on axial bottom slope, tidal intensity and constituents. Continental Shelf Research, 167: 1–13, doi: 10.1016/j.csr.2018.07.011

Cheng Peng, De Swart H E, Valle-Levinson A. 2013. Role of asymmetric tidal mixing in the subtidal dynamics of narrow estuaries. Journal of Geophysical Research: Oceans, 118(5): 2623–2639, doi: 10.1002/jgrc.20189

Cheng Peng, Mao Jianshan, Yu Fengling, et al. 2019. A numerical study of residual flow induced by eddy viscosity-shear covariance in a tidally energetic estuary. Estuarine, Coastal and Shelf Science, 230: 106446

Cheng Peng, Valle-Levinson A, De Swart H E. 2010. Residual currents induced by asymmetric tidal mixing in weakly stratified narrow estuaries. Journal of Physical Oceanography, 40(9): 2135–2147, doi: 10.1175/2010JPO4314.1

Cheng Peng, Valle-Levinson A, De Swart H E. 2011. A numerical study of residual circulation induced by asymmetric tidal mixing in tidally dominated estuaries. Journal of Geophysical Research: Oceans, 116(C1): C01017

Cheng Peng, Wilson R E. 2008. Modeling sediment suspensions in an idealized tidal embayment: Importance of tidal asymmetry and settling lag. Estuaries and Coasts, 31(5): 828–842, doi: 10.1007/s12237-008-9081-4

Cheng Peng, Yu Fengling, Chen Nengwang, et al. 2020. Observational study of tidal mixing asymmetry and eddy viscosity-shear covariance–induced residual flow in the Jiulong River estuary. Continental Shelf Research, 193: 104035, doi: 10.1016/j.csr.2019.104035

Chernetsky A S, Schuttelaars H M, Talke S A. 2010. The effect of tidal asymmetry and temporal settling lag on sediment trapping in tidal estuaries. Ocean Dynamics, 60(5): 1219–1241, doi: 10.1007/s10236-010-0329-8

Dijkstra Y M, Schuttelaars H M, Burchard H. 2017. Generation of exchange flows in estuaries by tidal and gravitational eddy viscosity-shear covariance (ESCO). Journal of Geophysical Research: Oceans, 122(5): 4217–4237, doi: 10.1002/2016JC012379

Dijkstra Y M, Schuttelaars H M, Schramkowski G P, et al. 2019. Modeling the transition to high sediment concentrations as a response to channel deepening in the Ems River Estuary. Journal of Geophysical Research: Oceans, 124(3): 1578–1594, doi: 10.1029/2018JC014367

Dyer K R. 1997. Estuaries: A Physical Introduction. 2nd ed. Chichester: John Wiley and Sons, 22–29

Fram J P, Martin M A, Stacey M T. 2007. Dispersive fluxes between the coastal ocean and a semienclosed estuarine basin. Journal of Physical Oceanography, 37(6): 1645–1660, doi: 10.1175/JPO3078.1

Friedrichs C T, Aubrey D G. 1994. Tidal propagation in strongly convergent channels. Journal of Geophysical Research: Oceans, 99(C2): 3321–3336, doi: 10.1029/93JC03219

Friedrichs C T, Hamrick J M. 1996. Effects of channel geometry on cross sectional variations in along channel velocity in partially stratified estuaries. In: Aubrey D G, Friedrichs C T, eds. Buoyancy Effects on Coastal and Estuarine Dynamics. Washington, D.C: American Geophysical Union, 53: 283–300

Fugate D C, Friedrichs C T, Sanford L P. 2007. Lateral dynamics and associated transport of sediment in the upper reaches of a partially mixed estuary, Chesapeake Bay, USA. Continental Shelf Research, 27(5): 679–698, doi: 10.1016/j.csr.2006.11.012

Geyer W R, MacCready P. 2014. The estuarine circulation. Annual Review of Fluid Mechanics, 46: 175–197, doi: 10.1146/annurev-fluid-010313-141302

Geyer W R, Scully M E, Ralston D K. 2008. Quantifying vertical mixing in estuaries. Environmental Fluid Mechanics, 8(5–6): 495–509, doi: 10.1007/s10652-008-9107-2

Geyer W R, Signell R P, Kineke G C. 1997. Lateral trapping of sediment in partially mixed estuary. In: Dronker J, Scheffers M, eds. Physics of Estuaries and Coastal Seas. The Hague, 115–124

Huijts K M H, Schuttelaars H M, De Swart H E, et al. 2006. Lateral entrapment of sediment in tidal estuaries: An idealized model study. Journal of Geophysical Research: Oceans, 111(C12): C12016, doi: 10.1029/2006JC003615

Huijts K M H, Schuttelaars H M, De Swart H E, et al. 2009. Analytical study of the transverse distribution of along-channel and transverse residual flows in tidal estuaries. Continental Shelf Research, 29(1): 89–100, doi: 10.1016/j.csr.2007.09.007

Jay D A, Musiak J D. 1994. Particle trapping in estuarine tidal flows. Journal of Geophysical Research: Oceans, 99(C10): 20445–20461, doi: 10.1029/94JC00971

Jiang Chenjuan, De Swart H E, Li Jiufa, et al. 2013. Mechanisms of along-channel sediment transport in the North Passage of the Yangtze Estuary and their response to large-scale interventions. Ocean Dynamics, 63(2): 283–305

Lacy J R, Monismith S G. 2001. Secondary currents in a curved, stratified, estuarine channel. Journal of Geophysical Research: Oceans, 106(C12): 31283–31302, doi: 10.1029/2000JC000606

Li Xiangyu, Geyer W R, Zhu Jianrong, et al. 2018. The transformation of salinity variance: A new approach to quantifying the influence of straining and mixing on estuarine stratification. Journal of Physical Oceanography, 48(3): 607–623, doi: 10.1175/JPO-D-17-0189.1

Li Lu, Wu Hui, Liu Jame T., et al 2015. Sediment transport induced by the advection of a moving salt wedge in the Changjiang Estuary. Journal of Coastal Research, 31(3): 671–679

Lin Jing, Kuo A Y. 2001. Secondary turbidity maximum in a partially mixed microtidal estuary. Estuaries, 24(5): 707–720, doi: 10.2307/1352879

Luan Hualong, Ding Pingxing, Wang Zhengbing, et al. 2017. Process-based morphodynamic modeling of the Yangtze Estuary at a decadal timescale: Controls on estuarine evolution and future trends. Geomorphology, 290: 347–364, doi: 10.1016/j.geomorph.2017.04.016

Manning A J, Bass S J. 2006. Variability in cohesive sediment settling fluxes: Observations under different estuarine tidal conditions. Marine Geology, 235(1–4): 177–192, doi: 10.1016/j.margeo.2006.10.013

Munk W H, Anderson E R. 1948. Notes on a theory of the thermocline. Journal of Marine Research, 7(3): 276–295

Scully M E, Friedrichs C T. 2003. The influence of asymmetries in overlying stratification on near-bed turbulence and sediment suspension in a partially mixed estuary. Ocean Dynamics, 53(3): 208–219, doi: 10.1007/s10236-003-0034-y

Scully M E, Friedrichs C T. 2007. Sediment pumping by tidal asymmetry in a partially mixed estuary. Journal of Geophysical Research: Oceans, 112(C7): C07028

Scully M E, Geyer W R. 2012. The role of advection, straining, and mixing on the tidal variability of estuarine stratification. Journal of Physical Oceanography, 42(5): 855–868, doi: 10.1175/JPO-D-10-05010.1

Simpson J H, Brown J, Matthews J, et al. 1990. Tidal straining, density

currents, and stirring in the control of estuarine stratification. Estuaries, 13(2): 125–132, doi: 10.2307/1351581

Stacey M T, Brennan M L, Burau J R, et al. 2010. The tidally averaged momentum balance in a partially and periodically stratified estuary. Journal of Physical Oceanography, 40(11): 2418–2434, doi: 10.1175/2010JPO4389.1

Stacey M T, Fram J P, Chow F K. 2008. Role of tidally periodic density stratification in the creation of estuarine subtidal circulation. Journal of Geophysical Research: Oceans, 113(C8): C08016

Talke S A, De Swart H E, Schuttelaars H M. 2009. Feedback between residual circulations and sediment distribution in highly turbid estuaries: An analytical model. Continental Shelf Research, 29(1): 119–135, doi: 10.1016/j.csr.2007.09.002

Tessier E, Garnier C, Mullot J U, et al. 2011. Study of the spatial and historical distribution of sediment inorganic contamination in the Toulon Bay (France). Marine Pollution Bulletin, 62(10): 2075–2086, doi: 10.1016/j.marpolbul.2011.07.022

Uncles R J, Stephens J A, Law D J. 2006. Turbidity maximum in the macrotidal, highly turbid Humber Estuary, UK: Flocs, fluid mud, stationary suspensions and tidal bores. Estuarine, Coastal and Shelf Science, 67(1–2): 30–52

Wang Chenglong, Zhao Yifei, Zou Xinqing, et al. 2017. Recent changing patterns of the Changjiang (Yangtze River) Estuary caused by human activities. Acta Oceanologica Sinica, 36(4): 87–96, doi: 10.1007/s13131-017-1017-z

Winterwerp J C. 2002. On the flocculation and settling velocity of estuarine mud. Continental Shelf Research, 22(9): 1339–1360, doi: 10.1016/S0278-4343(02)00010-9

Yang Zhongyong, De Swart H E, Cheng Heqin, et al. 2014. Modelling lateral entrapment of suspended sediment in estuaries: The role of spatial lags in settling and M_4 tidal flow. Continental Shelf Research, 85: 126–142, doi: 10.1016/j.csr.2014.06.005

Yang Zhongyong, Wang Zhong, Cheng Heqin, et al. 2017. Analytical study of the sediment transport in the South Channel of Yangtze estuary, China. Haiyang Xuebao (in Chinese), 39(5): 22–32

Yu Qian, Flemming B W, Gao Shu. 2011. Tide-induced vertical suspended sediment concentration profiles: phase lag and amplitude attenuation. Ocean Dynamics, 61(4): 403–410, doi: 10.1007/s10236-010-0335-x

Appendix A: Decomposition of the governing equations

The equation of hydrodynamics can be decomposed into dominant order (represent tidal flow), and first order (represent residual flow). The governing hydrodynamic equations in dominant order (i.e., M_2 tidal flow u_2) becomes

$$\frac{\partial u_2}{\partial t} = -g\frac{\partial \eta_2}{\partial x} + \frac{\partial}{\partial z}\left(A_0\frac{\partial u_2}{\partial z}\right). \tag{A1}$$

Boundary conditions for u_2 at the surface and at the bottom are similar to Eqs (2c) and (2d). The discharge per unit width is q_2, i.e.,

$$\int_{-H}^{0} u_2 \mathrm{d}z = q_2. \tag{A2}$$

The governing equations in first order (u_0) becomes

$$0 = \frac{g}{\rho_0}\frac{\partial \rho}{\partial x}z - g\frac{\partial \eta_0}{\partial x} + \frac{\partial}{\partial z}\left(A_0\frac{\partial u_0}{\partial z}\right) + \left\langle \frac{\partial}{\partial z}\left(A_2\frac{\partial u_2}{\partial z}\right)\right\rangle. \tag{A3}$$

Angle brackets denote average values over a tidal period. Three components of residual flow are considered in our model, that are driven by the horizontal density gradient $\left(\frac{g}{\rho_0}\frac{\partial \rho}{\partial x}z\right)$, by the asymmetry of tidal mixing $\left\langle \frac{\partial}{\partial z}\left(A_2\frac{\partial u_2}{\partial z}\right)\right\rangle$, and by fresh water discharge (q_0), respectively ($u_0 = u_{0\rho} + u_{0a} + u_{0q}$). Their governing equations are

$$0 = \frac{g}{\rho_0}\frac{\partial \rho}{\partial x}z - g\frac{\partial \eta_{0\rho}}{\partial x} + \frac{\partial}{\partial z}\left(A_0\frac{\partial u_{0\rho}}{\partial z}\right), \tag{A4}$$

$$0 = -g\frac{\partial \eta_{0a}}{\partial x} + \frac{\partial}{\partial z}\left(A_0\frac{\partial u_{0a}}{\partial z}\right) + \left\langle \frac{\partial}{\partial z}\left(A_2\frac{\partial u_2}{\partial z}\right)\right\rangle, \tag{A5}$$

$$0 = -g\frac{\partial \eta_{0q}}{\partial x} + \frac{\partial}{\partial z}\left(A_0\frac{\partial u_{0q}}{\partial z}\right). \tag{A6}$$

Boundary conditions at surface and bottom for each component are similar to Eqs (2c) and (2d). However, the width unit discharge for $u_{0\rho}$ and u_{0a} is 0, but for u_{0q} is q_0, i.e.,

$$\int_{-H}^{0} (u_{0\rho}, u_{0a})\mathrm{d}z = 0, \tag{A7}$$

$$\int_{-H}^{0} u_{0q}\mathrm{d}z = q_0. \tag{A8}$$

The equation of sediment dynamics can be decomposed into dominant order (c_0 and c_4), which driven by dominant tidal flow, and first order (c_2), which is driven by residual flow in the first order system, i.e., $c = c_0 + c_2 + c_4$. Analogously, the near bottom reference sediment concentration can be decomposed into $c_a = c_{a0} + c_{a2} + c_{a4}$ due to the decomposition of near bottom shear stress. By applying perturbation techniques, the equation governing the mean SSC (c_0) is

$$w_s\frac{\partial c_0}{\partial z} + K_0\frac{\partial^2 c_0}{\partial z^2} = 0. \tag{A9}$$

The equation of M_2 SSC (c_2) reads

$$\frac{\partial c_2}{\partial t} - w_s\frac{\partial c_2}{\partial z} - K_0\frac{\partial^2 c_2}{\partial z^2} - K_2\frac{\partial^2 c_0}{\partial z^2} = 0. \tag{A10}$$

The M_2 SSC can be decomposed into two components, the first is driven by the M_2 part of the bottom shear stress, and the second is driven by the asymmetry of diffusivity, i.e., $c_2 = c_{2t} + c_{2a}$.

The governing equation of M_4 SSC (c_4) is

$$\frac{\partial c_4}{\partial t} - w_s \frac{\partial c_4}{\partial z} - K_0 \frac{\partial^2 c_4}{\partial z^2} = 0. \tag{A11}$$

The M_4 SSC is driven by the M_4 component of the bottom shear stress (c_4). All boundary conditions of hydrodynamics and sediment dynamics are decomposed into dominant order and first order with perturbation analysis, respectively. Therefore, the analytical solution of each flow and SSC component can be solved from the decomposed linear equations.

At last, the vertical profile of sediment flux (F) per unit width is obtained as the averaged product uc over a tidal cycle (P),

$$F = \frac{1}{P}\int_0^P uc\mathrm{d}t. \tag{A12}$$

The sediment flux is decomposed into several components since both u and c are composed of several parts:

$$F = \frac{1}{P}\int_0^P (u_0 + u_2)(c_0 + c_2)\,\mathrm{d}t = \frac{1}{P}\int_0^P (u_0 c_0 + u_2 c_2)\,\mathrm{d}t = F_0 + F_2. \tag{A13}$$

Here, the residual sediment flux (F_0) is decomposed into $F_{0\rho}$ (horizontal density gradient induced residual sediment flux), F_{0a} (asymmetric tidal mixing induced residual sediment flux), and F_{0q} (fresh water discharge induced sediment flux), i.e.,

$$F_0 = \frac{1}{P}\int_0^P \left(u_{0\rho} + u_{0a} + u_{0q}\right) c_0 \mathrm{d}t = F_{0\rho} + F_{0a} + F_{0q}. \tag{A14}$$

The tidal sediment flux can be decomposed into F_{2t} (asymmetric bottom shear stress induced sediment flux), and F_{2a} (asymmetric diffusivity induced sediment flux), i.e.,

$$F_2 = \frac{1}{P}\int_0^P u_2 (c_{2t} + c_{2a})\,\mathrm{d}t = F_{2t} + F_{2a}. \tag{A15}$$

The sediment transport per unit width (T) is obtained by integrating the vertical profile of sediment flux over depth,

$$T = \int_{-H}^0 F\mathrm{d}z. \tag{A16}$$

It is split into three mean transport components (T_0) and two tidal transport components (T_2), with each term has the similar meaning to that of sediment flux terms,

$$T = T_0 + T_2 = \left(T_{0\rho} + T_{0a} + T_{0q}\right) + \left(T_{2t} + T_{2a}\right). \tag{A17}$$